1-1-2014

A study of plastic deformation behavior during high pressure torsion process by crystal plasticity finite element simulation

Peitang Wei
University of Wollongong, pw023@uowmail.edu.au

Cheng Lu
University of Wollongong, chenglu@uow.edu.au

A K. Tieu
University of Wollongong, ktieu@uow.edu.au

Guanyu Deng
University of Wollongong, gdeng@uow.edu.au

A study of plastic deformation behavior during high pressure torsion process by crystal plasticity finite element simulation

Abstract

High pressure torsion (HPT) is an efficient technique of producing ultrafine grained materials with exceptional small grain size. In this study, a crystal plasticity finite element method (CPFEM) model has been developed to investigate the plastic deformation behavior of pure aluminum single crystal during the HPT process. The simulation results show that, the distribution and evolution of the macroscopic plastic strain and the accumulative shear strain are similar. The value increases with the increase of the distance from the center as well as the number of revolution. The simulation is capable of reflecting the anisotropic characteristics of HPT deformation, a non-homogenous deformation along the circumference of the sample could be observed. At the early stage of HPT deformation, the critical resolved shear stress (CRSS) along the radial direction presents a rapid increase, followed by a moderate increase and then reaches the near-saturate state. As the HPT deformation proceeds, there is a relatively weak increase in the quasi-saturate value and the near-steady region expands gradually towards the sample center. The orientation changes during the HPT process with increasing applied strain predicted by the developed CPFEM model are also presented.

Keywords

high, plastic, pressure, study, torsion, process, crystal, deformation, plasticity, behavior, finite, element, simulation, during

Disciplines

Engineering | Science and Technology Studies

Publication Details

Wei, P. T., Lu, C., Tieu, K. & Deng, G. Y. (2014). A study of plastic deformation behavior during high pressure torsion process by crystal plasticity finite element simulation. IOP Conference Series: Materials Science and Engineering, 63 012045-1-012045-11.

A study of plastic deformation behavior during high pressure torsion process by crystal plasticity finite element simulation

2014 IOP Conf. Ser.: Mater. Sci. Eng. 63 012045

(http://iopscience.iop.org/1757-899X/63/1/012045)

IOP Conf. Series: Materials Science and Engineering **63** (2014) 012045 doi:10.1088/1757-899X/63/1/012045

A study of plastic deformation behavior during high pressure torsion process by crystal plasticity finite element simulation

P T Wei, C Lu, K Tieu, G Y Deng

School of Mechanical, Materials and Mechatronic Engineering,
University of Wollongong, Wollongong, NSW 2522, Australia
E-mail: pw023@uowmail.edu.au

Abstract. High pressure torsion (HPT) is an efficient technique of producing ultrafine grained materials with exceptional small grain size. In this study, a crystal plasticity finite element method (CPFEM) model has been developed to investigate the plastic deformation behavior of pure aluminum single crystal during the HPT process. The simulation results show that, the distribution and evolution of the macroscopic plastic strain and the accumulative shear strain are similar. The value increases with the increase of the distance from the center as well as the number of revolution. The simulation is capable of reflecting the anisotropic characteristics of HPT deformation, a non-homogenous deformation along the circumference of the sample could be observed. At the early stage of HPT deformation, the critical resolved shear stress (CRSS) along the radial direction presents a rapid increase, followed by a moderate increase and then reaches the near-saturate state. As the HPT deformation proceeds, there is a relatively weak increase in the quasi-saturate value and the near-steady region expands gradually towards the sample center. The orientation changes during the HPT process with increasing applied strain predicted by the developed CPFEM model are also presented.

1. Introduction

Severe plastic deformation (SPD) processes are capable of achieving relatively high strains without introducing any major changes in the sample shape. SPD has attracted numerous interest in fabrication of ultrafine grained (UFG) materials over the last two decades [1,2]. The grains produced by SPD are significantly smaller than those produced by conventional metal-processing techniques, having size in sub-micrometer or even nanometer range. Several different SPD processing techniques are available, including equal channel angular pressing (ECAP), accumulative roll bonding (ARB) and HPT, etc. Compared with other SPD methods, investigations suggest that HPT can permit a continuous strain in a very simple way without changing the working condition and is especially effective for producing exceptional grain refinement. Materials processed by HPT show some excellent properties, such as, ultrahigh strength, low temperature and/or high strain rate super-plasticity, enhanced fatigue behavior and superior corrosion resistance [3].

The principle of HPT processing has been depicted schematically in Ref. [3]. A disk-shape sample is usually deformed by simple shear between two anvils, which rotate with respect to one another under the pressure of several GPa. When the disk is deformed in torsion, the imposed equivalent strain, ε_{eq}, can be calculated by

$$\varepsilon_{eq} = \frac{2\pi Nr}{\sqrt{3}h} \quad (1)$$

where N is the number of turns, r is the distance from the center of the disk sample and h is the thickness of the disk sample.

Recently, a great deal of researches were devoted to numerical simulation of the HPT process, such as, Kim et al. [4,5], Rosochowski et al. [6], Busquet et al. [7], Lapovok et al. [8], Figueiredo et al. [9,10], Verleysen et al. [11] and Wei et al. [12]. All of these simulations were carried out using classical finite element method (FEM) and the simulated materials behaved as elastic-plastic isotropic work-hardening solids. The simulation results have presented some plastic deformation characteristics of the HPT process, such as, the material flow characteristics, the distributions and evolutions of mean normal stress, equivalent strain and strain rate, and the sample geometry after deformation.

In the past few years, various crystal plasticity models including classical Taylor type models and Visco-plastic Self-Consistent (VPSC) models have been established to simulate very

large strain torsion deformation [13–23]. The Taylor-type model assumes that the local strain rate is equal to the macroscopic strain rate, while the VPSC model allows the strain rate of each grain to be different from not only the macroscopic strain rate but also those of neighboring grains. In these crystal plasticity models for large strain torsion deformation, different hardening laws were adopted. In the models used in [15, 17, 21], slip systems hardening due to deformation was not considered, the CRSS was assumed to be constant. Toth et al.'s model [18] adopted simple isotropic hardening at slip level and the CRSS-shear strain curve was gave. Duchene et al.'s model [20] employed a simple power-type hardening law. In the models used in [16, 22], the hardening of the slip systems was achieved by giving the specific values of CRSS at different deformation levels. Weerasooriya's model [13] used the hardening modulus defined by Asaro and Needleman.

Crystal plasticity simulations performed for the HPT process are relatively limited. Hafok and Pippan [24] constructed a fully-constrained Taylor model for HPT. Kratochvil and his co-workers [25, 26] proposed a crystal plasticity model to explore the deformation mechanism during the HPT process which was assumed as uniform deformation of plane-strain double slip. Kratochvil et al.'s model was rate-independent and the hardening matrix components were taken as given material parameters. Draï and Aour [27] established a phenomenon-logical constitutive model based upon the Norton-Hoff flow rule to study the plastic deformation behavior in HPT. Draï et al.'s model incorporated the initial linear response, the non-linear response and the rate-dependence yield stress. They employed a simple hardening evolution law where the hardening variable R was defined relating with the macroscopic equivalent plastic strain ε^p and initial yield strain ε^0, $\mathrm{R} = (1 + \frac{\varepsilon^p}{\varepsilon^0})^m$.

In this paper, a CPFEM model, which incorporates crystal plasticity constitutive equations into a finite element framework, has been developed to simulate the deformation process of HPT. The CPFEM model provides a more accurate insight into the heterogeneities deformation among and within the grains. It has been demonstrated that the CPFEM model performed better than the Taylor and VPSC model for simulating the plastic deformation of crystalline materials [28–30]. Using the developed CPFEM model, the plastic deformation characteristics of aluminum single crystal during the HPT process will be analyzed in the paper.

2. Simulation procedure

Details with regarding to the crystal plasticity theory and constitutive relations used in this paper could be found in Ref [31]. In the past decades, different hardening models have been developed since the evolution of crystal plasticity theory, Taylor [32, 33] proposed isotropic hardening moduli for single crystals. Peirce, Asaro and Needleman [34] proposed a model providing latent hardening, while for self-hardening they used the mathematical property of hyperbolic secant function to reach a peak of hardening and then saturate. Bassani and Wu [35, 36] proposed a particular multiplicative form of hardening law in which each diagonal component is taken as the product of a self-hardening term $\mathrm{F}(\gamma^\alpha)$ and an interactive term *G*:

$$\mathrm{h}_{\alpha\alpha} = \mathrm{F}(\gamma^\alpha)\mathrm{G} \tag{2}$$

where

$$\mathrm{F}(\gamma^\alpha) = (h_0 - h_s)\mathrm{sech}^2\left(\frac{(h_0 - h_s)\gamma^\alpha}{\tau_1 - \tau_0}\right) + h_s \tag{3}$$

$$\mathrm{G} = 1 + \sum_{\substack{\beta=1 \\ \beta\neq\alpha}}^{N} f_{\alpha\beta} \tanh\left(\frac{\gamma^{(\beta)}}{\gamma_0}\right) \tag{4}$$

And the off-diagonal components are given by

$$h_{\beta\alpha} = \mathrm{q}h_{\alpha\alpha} \qquad \alpha \neq \beta \tag{5}$$

Where $h_{\alpha\alpha}$ is self-hardening moduli and $h_{\beta\alpha}$ denotes latent hardening moduli, q is a latent hardening parameter, h_0, h_s, τ_0 and τ_1 is hardening moduli and shear stress after initial yield and during easy sliding stage, γ^α is the accumulative shear strain on the particular slip system α, γ_0 represents the amount of slip after which the interaction between slip system α and β reaches peak strength, $f_{\alpha\beta}$ is the interaction parameter between two slip systems α and β.

$F(\gamma^{\alpha})$ gives a monotonically decreasing modulus at small strains and a finite rate of hardening at large γ^{α}. G equals unity while its arguments are all zero and approaches asymptotically to finite value when all slips $\gamma^{\beta}(\beta \neq \alpha)$ are large. It's worth noting that, since γ^{α} stands for the accumulative shear strain on the particular slip system α, i.e. $\int|\dot{\gamma^{\alpha}}|dt$, any component of the hardening matrix is inherently positive, therefore material softening was not considered.

The Bassani and Wu hardening law has been widely used in the crystal plasticity modellings of the large deformation processes, including ECAP [30, 37] and large strain torsion [38, 39]. In this study, the hardening model of Bassani & Wu was used, we modified the user material subroutine (UMAT) framework initially developed by Huang [40] and incorporated Bassani & Wu hardening model in the UMAT.

In this study, a series of material parameters need to be determined including $n, \dot{\gamma_0}, h_0, h_{s,}\tau_1, \tau_0, \gamma_0$ and slip interaction parameters a_1-a_5. Franciosi [41] obtained the slip system interaction parameters a_1-a_5 by conducting the latent hardening experiment using aluminum single crystal. The other parameters were identified by fitting the simulated stress-strain curve with the experimental results of single crystal aluminum under plane strain compression [42, 43]. The parameters adopted in this study are listed in Tab. 1. For the FCC crystals, we considered the {111}<110> slip systems where the crystallographic planes are defined by the {111} plane normal ($m^{(\alpha)}$) and the slip directions by the (110) slip vector ($s^{(\alpha)}$).

Table 1 Parameters in the hardening model

n	$\dot{\gamma_0}$ (1/s)	h_0 (MPa)	h_s (MPa)	τ_1 (MPa)	τ_0 (MPa)	γ_0	a_1	a_2	a_3	a_4	a_5
300	0.0001	100	0.01	6.3	6	0.001	1.75	1.75	1.75	2	2.25

The CPFEM simulation of the HPT process was constructed using the commercial finite element code ABAQUS 6.9-1. In the simulation, the sample had the initial dimension of 10 mm in diameter and 0.8 mm in thickness. The simulated material was pure aluminum single crystal with the elastic moduli of C_{11}=112,000 MPa, C_{12}=66,000 MPa and C_{44}=28,000 MPa. Two coordinate systems, global system C_g (X, Y, Z) and local system C_l (R, θ, Z), were established, as shown in Fig. 1a. The local R, θ and Z axes represents the radial, circumferential and axial directions at a given location in the global system, respectively. The global coordinate system was used in the simulation, while the local coordinate system was often used in the data analysis. The starting material was oriented with [001] crystallographic direction lying parallel to the Z axis and [100] lying parallel to the X axis of the global system C_g. The value φ in Fig. 1a stands for the angular displacement of the material point away from the fixed X axis on the shear plane. The initial orientation of the single crystal in the C_l coordinate system is as a function of φ, as is shown in Fig. 1c-1i. The initial orientations were represented by the black dots in the {111} pole figures. The horizontal and vertical axis of the pole figures stands for tangential and axial direction, respectively.

The type of elements used in the simulation was C3D8R. Enhanced hourglass control, which provides an increased resistance to the hourglassing problem and a more accurate displacement solution, was used in the simulation. There were 23,600 elements and 26,895 nodes used in the simulation, which gave ten layers of elements along the thickness direction (see Fig. 1b). In the HPT simulation, the mesh was strongly distorted due to large torsion deformation so that the simulations became unstable or breakdown. In order to solve this problem, mesh-to-mesh solution mapping technique built in ABAQUS was employed. A regular mesh was initially used. After a pre-determined revolution, the simulation was stopped. A new mesh for the deformed sample was consequently generated. Mesh-to-mesh solution mapping technique was used to transfer all state variable values from old mesh to new mesh. The simulation then re-started and the above procedure was repeated until the desired deformation was reached. The efficiency of the mapping method has been examined in a previously published paper [12].

In the simulation, the up and lower anvils were regarded as a whole of rigid body to constrain the radial movement of the side surface of the sample, as is depicted schematically in Fig. 1a. The radius of the rigid body was 5.01mm. The axial and tangential displacement of bottom surface of the sample was fixed and the top surface of the sample was rotated to a torsion angle of 90° under the pressure of about 1 GPa. The relative movement between the side surface of the sample and the rigid body is allowed in the simulation. The coefficient of friction for the contact between the side surface of the sample and the rigid body was assumed to be 0.1, which is a generally used value for the cold metal forming processes without lubrication.

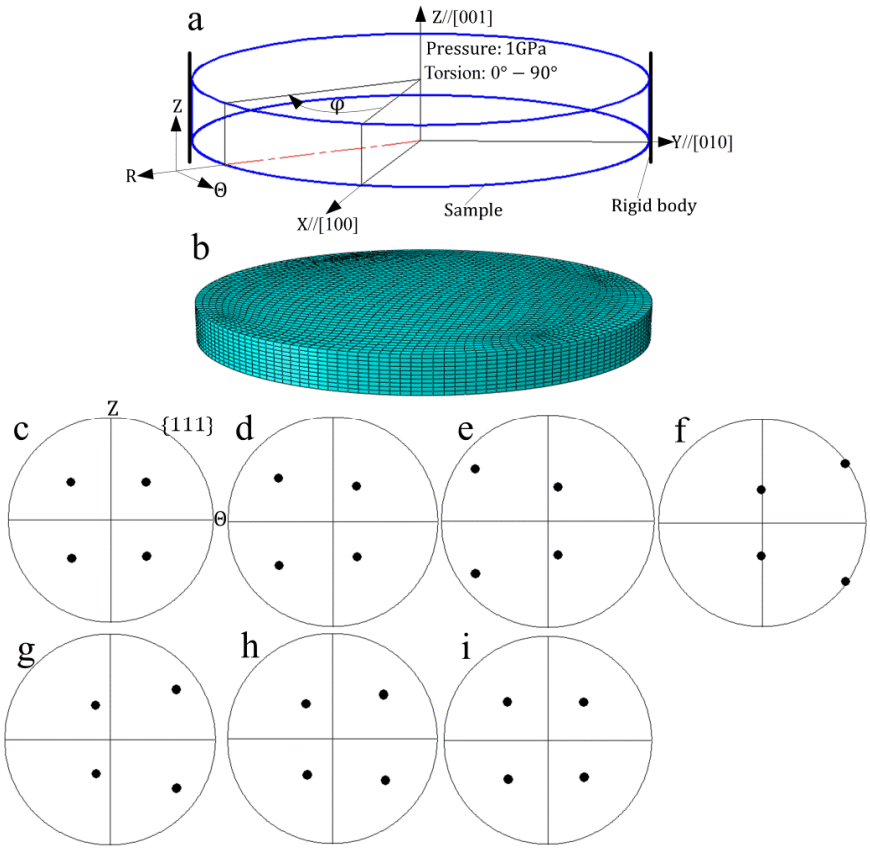

Fig. 1 The CPFEM model of the HPT process. a, The sample and the rigid body. b, Initial finite element mesh of the sample. c-i, initial orientation as a function of φ, c, φ = 0°, d, φ = 15°, e, φ = 30°, f, φ = 45°, g, φ = 60°, h, φ = 75°, i, φ = 90°.

3. Results and discussion

Hafok and Pippan [44] experimentally investigated the deformation homogeneity in HPT. Fig. 2a shows the grid cut on the sample surface by a FIB device before the HPT deformation in Hafok and Pippan's experiment. As shown in Fig. 2b, after the deformation all structure elements were sheared by almost the same amount (a uniform shear deformation), which indicated the microstructure was deformed homogeneously.

Fig. 2c shows the simulated mesh on the side surface of the sample subjected to the pressure of 1 GPa and torsion angle of 30°. It can be seen that all horizontal lines remain straight and are perpendicular to the axial direction, while the vertical lines have a certain angle with the Z direction and these lines are almost parallel to each other, implying a homogenous deformation across the sample thickness.

Fig. 2d illustrates the distribution of displacement recorded on the half sample after the HPT deformation with the pressure of 1 GPa and torsion angles of 30°. Two obvious material flow characteristics could be observed. Firstly, the higher level of displacement locates at the pe-

riphery of the sample and it decreases while approaching the center of the sample. Moreover, since during the process of HPT the top surface of the sample is rotated to apply the torsion strain and the bottom surface remains static, the pronounced displacement gradient could be induced along the thickness direction and it is more obvious around the edge region of the sample.

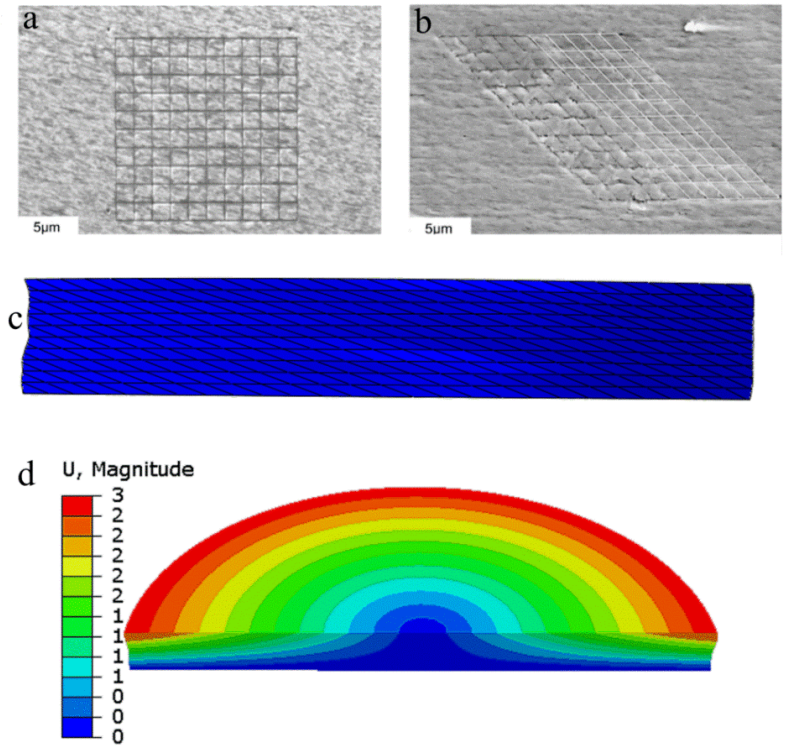

Fig. 2 a-b, Grid on the surface of the sample before and after HPT deformation (experimentally observed by Hafok and Pippan). c, Deformation of mesh on the side surface of the sample after pressure of 1 GPa and torsion angle of 30°. d, Distribution of the simulated displacement on the half sample after pressure of 1 GPa and torsion angle of 30°

Since the mechanical properties of the materials are directly relevant to the development of plastic deformation induced to the sample, the plastic strain during the HPT process is worth a close examination using the CPFEM simulation. Figs. 3a~3c show the distributions of true strain on the top surface of HPT deformed sample subjected to the torsion angles of 30°, 60° and 90°, respectively. It can be seen that, when the sample is deformed by the revolution angle of 30°, the strain remains relatively small at the sample center and it increases with the distance from the sample center. The maximum strain located at the edge of the sample is around 1.4. The strain increase as the number of revolution increases. The lowest strain at the disk centers and highest strain at the edges are always observed. The highest values are 2.8 and 4.2 for the revolution angles of 60° and 90°, respectively, as shown in Fig. 3b and 3c. These results are similar to those obtained by the classical FEM simulations of HPT [9, 10, 12]. After conducting close comparisons of the results between the CPFEM and the classical FEM, it's found that there are slightly differences in the strain distribution on the sample surface. The FEM simulations gave a homogenous distribution along the circumference of the surface, while by using the CPFEM, the deformation is non-homogenous along the circumferential direction. It can be found from Fig. 3 that a distribution pattern with four-fold symmetry, namely four more strained regions separated by four less-strained regions, could be observed, particularly around the periphery region. This finding is consistent with the previously published works [45,46], which illustrated that the torsion deformation of a tubular sample with respect to a [001] axis was associated with the formation of four zones of intense deformation.

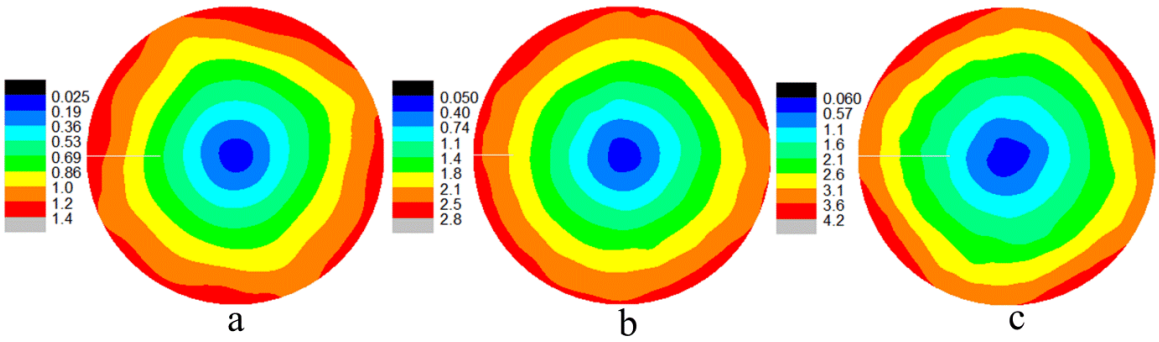

Fig. 3 The distribution of true strain on the surface of HPT deformed disk with pressure of 1 GPa and torsion angle of a, 30°, b, 60° and c 90°.

It has been well known that the crystallographic slip is the major plastic deformation mechanism. In this study, the slip activities including the evolution of the accumulative shear strains and the hardening behavior during the HPT process are investigated by using CPFEM simulation.

Fig. 4 illustrates the distribution of the accumulative shear strain on the top surface of HPT deformed disk for the torsion angle of 30°, 60° and 90°, respectively. Similar to the plastic strain described in Fig. 3, the higher shear strain is located at the periphery region and it decreases from the edge of the sample to the center. The non-uniform distribution along the tangential direction, especially at the region close to the sample edge, is also observed.

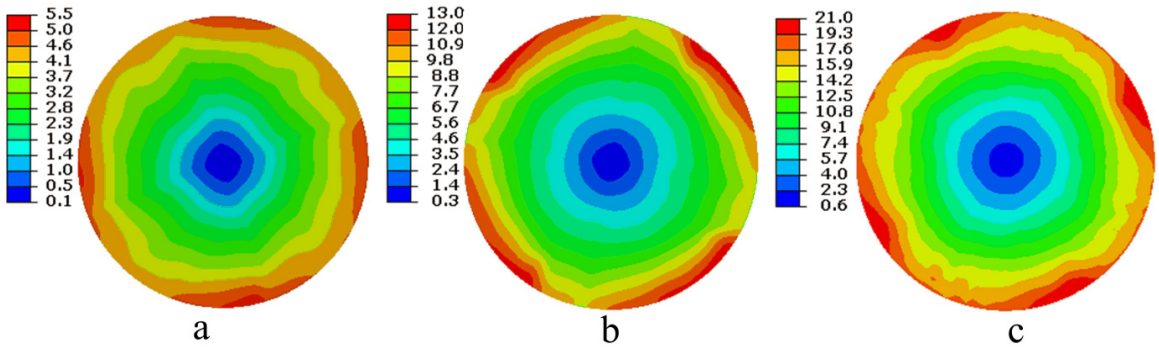

Fig. 4 The distribution of accumulative shear strain on the surface of HPT deformed disk with pressure of 1 GPa and torsion angle of a, 30°, b, 60° and c 90°.

In order to investigate the evolution of the accumulative shear strain, different referential paths are defined on the top surfaces of the HPT deformed disks with rotation angles from 15° to 90°. The paths spread from the sample center to the most strained edge region. Fig. 5 illustrates the simulation results of the accumulative shear strain recorded on the predefined paths. It can be seen from Fig. 5 that at the early stage of HPT deformation, 15° torsion, the accumulative slip strain is very small in the region close to the sample center and it increases slightly from the sample center to the edge. As the HPT deformation continues, after 30° and 45°torsion, the accumulative shear strain around the sample center still remains low and there is an approximate linear increase away from the center. For the higher torsion angles a slightly higher increase rate at the region with radius> 3.5 mm can be observed.

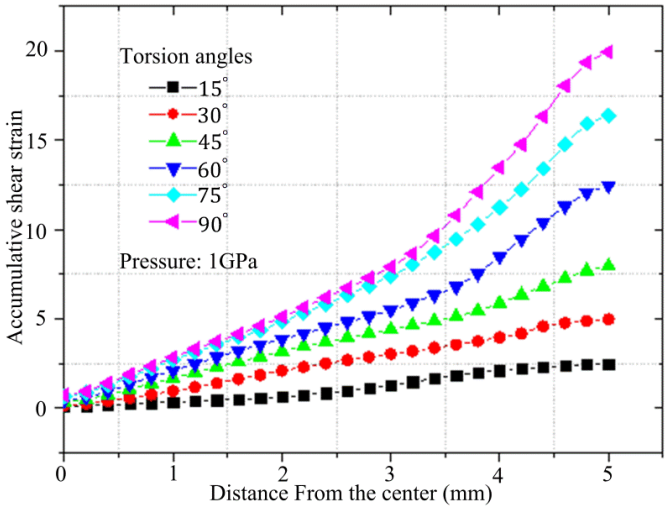

Fig. 5. The accumulative shear strain as a function of the distance from the sample center after different torsion angle from 15° to 90°.

Figs. 6a~6c illustrate the distribution of the CRSS on the top surface of HPT deformed disk for the torsion angles of 30°, 60° and 90°, respectively. In Fig. 6a, after the 30° HPT deformation, at the region with radius < 2mm, the hardening has already launched with the minimum CRSS of 17 MPa. For the region with radius > 2mm, it's clear that the CRSS presents the non-uniform distribution along the circumferential direction. Four regions with intense hardening are separated by four regions with relatively gentle hardening.
When the deformation proceeds, as can be seen in Fig. 6b and c, the CRSS increases, indicating that the further hardening has happened. It's worth noting that as the torsion increases from 15° to 90°, the minimum value of CRSS increases significantly from 17 MPa to around 27 MPa, while the maximum value presents only a slight increase from 58 MPa to around 60 MPa. It has been also observed that the region with the higher CRSS expands towards the sample center, leading to that the region around the sample center with less hardening shrinks. In addition, the non-uniform hardening along the tangential direction could be observed in Fig.6 for all the torsion angles.

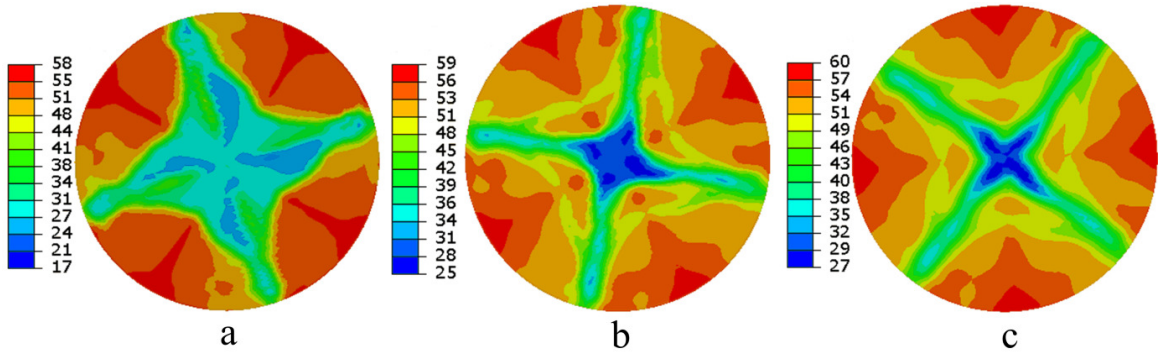

Fig. 6 The distribution of current strength in slip systems on the surface of HPT deformed disk with pressure of 1 GPa and torsion angle of a, 30°, b, 60° and c 90°.

In order to examine the hardening behavior with increasing applied torsion strain, different referential paths are defined on the top surfaces of HPT deformed disks with torsion angle from 15° to 90°. The paths spread from the sample centers to the edge regions with the largest CRSS. Fig. 7 shows the simulation results of the CRSS following the pre-defined paths. It can be seen from Fig. 7 that, after the 15° torsion deformation, at the region of radius < 4 mm, the CRSS has a nearly constant value of around 30 MPa. At the region of radius between 4 mm and 4.7 mm, the current strength increases significantly, indicating a rapid

hardening in this region. At the region close to the edge, the CRSS presents a moderate increase.

As the HPT deformation proceeds, the CRSS still remains a leveling-off at around 30 MPa at the region close to sample center. Beyond the leveling-off region the CRSS always increases significantly with the distance from the sample center, followed by a gentle increase and then reaches a near-steady state. In addition, with the increasing applied torsion strain, for the near-steady region, only a weak increase in the CRSS could be observed. There is a tendency that the near-steady region expands gradually towards the sample center, accordingly the range of the leveling-off region around the sample center becomes smaller as the torsion angle increases.

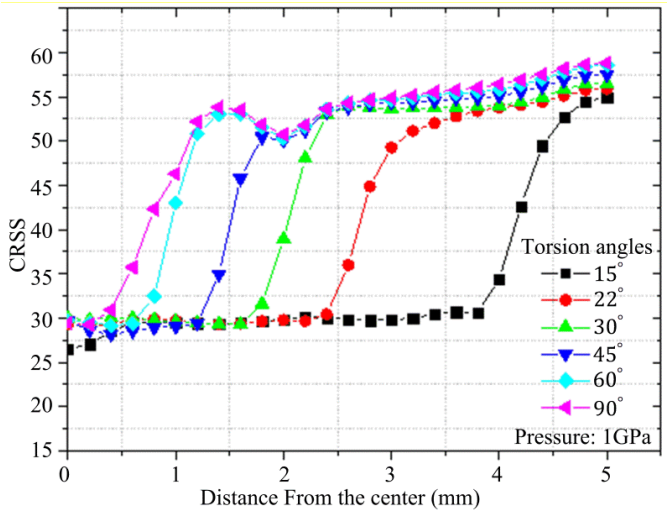

Fig. 7 The CRSS as a function of the distance from the sample center after different torsion angle from 15° to 90°.

In order to investigate the orientation changes during the HPT process, when the sample is un-deformed, a small region at the periphery of the sample along the X direction of the top surface is selected. The center of the selected region is X=4.75mm, Y=0mm and Z=0.7mm. Its initial orientation in the local coordinate system C_l is the near-cube orientation, as shown in Fig. 8a. As the material is deformed continuously by the shear strain, the selected region flows around the torsion axis with respect to X axis on the shear plane simulating the crystallographic orientation changes. The resulting orientations with increasing applied strain predicted by the developed CPFEM model are presented in Fig. 8 by means of {111} pole figures. The pole figures are all recorded on the $\theta - Z$ plane. The main torsion texture components are listed and their locations on the {111} pole figures are visualized by different symbols. The obtained orientations are marked by black dots.

The effect of the increasing shear strain on the orientation changes is initially illustrated in Fig. 8b with the 30° revolution angle. The poles rotate significantly away from their initial positions due to the continuous lattice rotations. The developed orientations locate around the position of the near rotated cube orientation which is not stable. Moreover, the orientations arrange as steak-like distribution in the pole figure. Fig. 8c shows the orientations of the selected region corresponding to 45° torsion deformation. The lattices are further rotated to accommodate the applied torsion strain and the orientations approach gradually to a certain crystallographic orientation. The steak-like distribution is elongated and becomes even more obvious. One can see from Fig. 8d that after the 85° torsion deformation, the selected region has the orientations predominated by the C component of the ideal torsion texture, which favors the alignment of {001} slip planes with the shear plane and $< 0\bar{1}1 >$ slip directions with the shear direction.

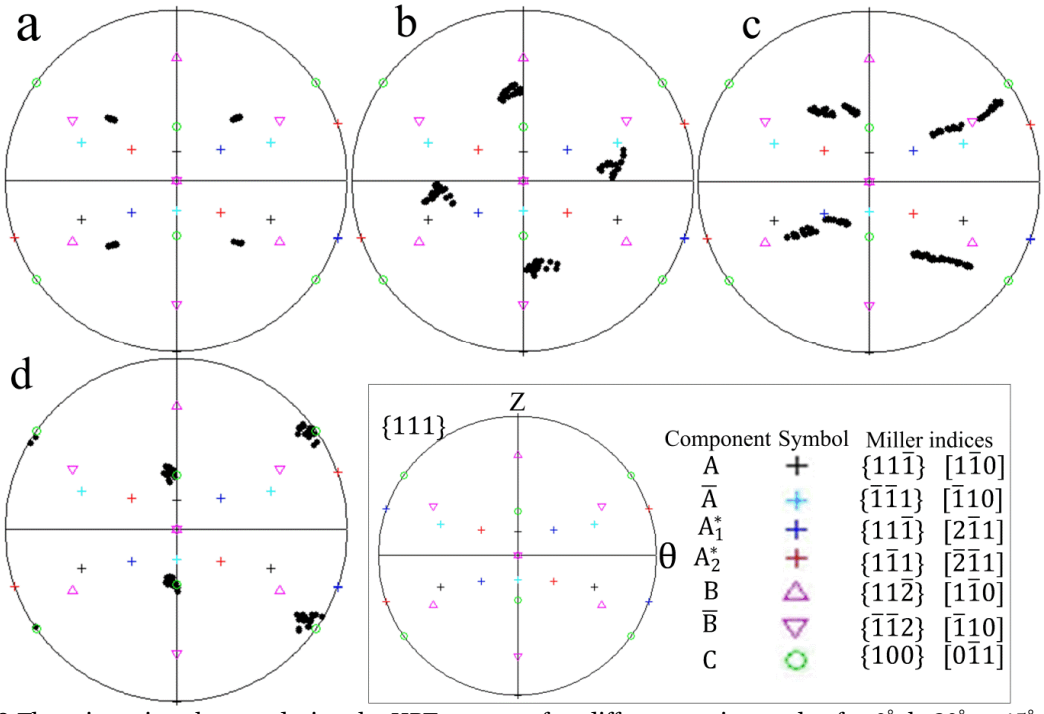

Fig. 8 The orientation changes during the HPT process after different torsion angle of a, 0°, b, 30°, c, 45° and d, 85°.

The results obtained for the evolution of local crystal orientation in the present work are in good coherence with the results that have been published previously for shear deformation. Indeed, the main deformation mode in the present HPT simulation locally is simple shear for which case the behavior of an initially cube oriented crystal is well documented. In 1968 Rose and Stüwe [47] published experimental results for initially strongly cube oriented textured tubes in torsion for copper. They have found that the texture was simply rotated with the rigid body rotation. The plastic deformation, however, was not large. In 1989 Toth and Jonas [48] showed by analytical modeling that in simple shear of cube orientation the plastic spin is zero so that the lattice spin is equal to the rigid body spin for any rotated position of the initially cube oriented crystal, therefore it rotates in the direction of the imposed rigid body rotation. The same result has been found in the present work, at least up to an imposed rotation angle of the disk by 30°, see Fig. 8b. At this position, the cube is rotated nearly by 45° around the radial axis, which is the axis of rigid body rotation in HPT. However, for larger rotations, the lattice spin becomes very different because the rotation does not take place any more around the rigid body rotation axis; the crystal orientations become slightly spread around the rotated position and they all rotate progressively into the C component of the ideal orientation of shear textures(Fig. 8d). Such rotation has also been observed and modeled previously for a Ni single crystal subjected to one pass Equal Channel Angular Extrusion [49]. In that study the Ni single crystal was oriented initially almost like the orientation in Fig. 8b with respect to the imposed deformation, which is mainly simple shear in ECAE. Starting from this orientation, the authors of Ref. [49] have found experimentally that the crystal rotates into the C component. It was also modeled by polycrystal simulations starting with a polycrystal with orientations near to the initial ideal position. Modeling by a cloud of grains instead of one single orientation was important because the exact ideal orientation would rotate precisely with the rigid body rotation and would not reach the C component. However, when a spread is considered around the ideal initial position just like in Fig. 8b here the main texture component becomes the C at large strains. Therefore, our simulation results have already been confirmed previously in Refs. [47-49]. Even if those results were obtained for other materials (Cu and Ni), they deform also with the same {111}<110> slip systems, which were used also in the present case, for Aluminum.

4. Conclusions

(1) In this paper, the plastic deformation behavior of aluminum single crystal deformed by HPT was investigated by a CPFEM model. During the simulation procedure, mesh-to-mesh solution mapping technique was used to prevent severe element distortion.
(2) At the early stage of HPT deformation, the simulation results show that the mesh on the side surface of the sample are deformed homogenously and a pronounced displacement gradient along the thickness direction could be observed.
(3) The distribution and evolution of the plastic strain on the sample surface were presented. It has been found that the plastic strain increases with the increase of the distance from the center as well as the number of revolution. A non-uniform distribution along the circumferential direction could be found, four namely more strained regions are observed to be separated by four less strained regions.
(4) By the CPFEM simulation, the slip activities including the evolution of accumulative shear strain and the hardening behavior during HPT process were analyzed. The distribution and evolution of the accumulative shear strain are found to be similar to that of the plastic strain. The distribution of the CRSS also presents the non-uniform hardening along the tangential direction. At the early stage of HPT deformation, the CRSS along the radial direction presents a rapid increase, followed by a gentle increase and then reaches the near-steady state. As the HPT deformation proceeds, a weak increase in the quasi-saturate value could be found and there is a tendency that the near-steady region expands gradually towards the sample center.
(5) The orientation changes during the HPT process with increasing applied strain predicted by the developed CPFEM model are presented which are in good coherence with the previously published results.

References

[1] Kawasaki M, Figueiredo R B, Langdon T G 2012 *J. Mater. Sci.* ***47*** *7719*
[2] Verlinden B 2005 *MJOM* **11** 165
[3] Zhilyaev A, Langdon T G 2008 *Prog. Mater. Sci.* **53** 893
[4] Kim H S, Hong S I, Lee Y S, et al. 2003 *J. Mater. Process Technol.* **142** 334
[5] Yoon S C, Horita Z, Kim H S 2008 *J. Mater. Process Technol.* **201** 32
[6] Rosochowski A et al. 2007 *Proc. Inst. Mech. Eng. Part L J. Mater. Des. Appl.* **221** 187
[7]Busquet M, Descartes S, Berthier Y 2009 *Tribol. Int.* **42** 1730
[8] Lapovok R, Pougis A., Lemiale V, et al. 2010 *J. Mater. Sci* .**45** 4554
[9] Figueiredo R B, Cetlin P R, Langdon T G 2011 *Mater. Sci. Eng. A* **528** 8198
[10] Figueiredo R B, Aguilar MTP, Cetlin P R, Langdon T G 2012 *J. Mater. Sci.* **47** 7807
[11] Verleysen P, Abeele F Van Den, Degrieck J 2013 *Simulia Community Conf.* (Chicago) p 1
[12] Wei P T, Lu C, Tieu K, et al. 2013 *Steel Res. Int.* **84** 1246
[13] T Weerasooriya 1998 Shear and axial stress response under loading of OFHC copper
[14] Graham S, Stock S R, Ferney V C, et al. 1998 *J Eng Mater Technol* **120** 197
[15] Hughes D A., Lebensohn R A., Wenk H R, Kumar a. 2000 *Proc R Soc A Math Phys Eng Sci* **456** 921
[16] Sanchez P, Pochettino a., Chauveau T, Bacroix B 2001 *J Nucl Mater* **298** 329
[17] Böhlke T, Bertram A, Krempl E 2003 *Int J Plast* **19** 1867
[18] Qods F, Tóth L S, Van Houtte P 2005 *Mater Sci Forum* **495-497** 1609
[19] Habraken a. M, Gerday a. F, Diouf B, Duchêne L 2007 *AIP Conf Proc* **907** 1478
[20] Duchêne L, El Houdaigui F, Habraken A M 2007 *Int J Plast* **23** 1417
[21] Beausir B, Tóth L S, Qods F, Neale K W 2009 *J Eng Mater Technol* **131** 011108
[22] Klöden B, Oertel C-G, Skrotzki W, Rybacki E 2009 *J Eng Mater Technol* **131** 011102
[23] Wang H, Wu Y, Wu P D, Neale K W 2010 *CMC* **503** 1
[24] Hafok M, Pippan R 2008 *Philos. Mag.* **88** 1857
[25] Kratochvil J, Kruzik M, Sedlacek R 2009 *Acta Mater.* **57** 739
[26] Kratochvil J, Kruzik M, Sedlacek R 2010 *Rev. Adv. Mater. Sci.* **25** 88
[27] Draï A, Aour B 2013 *Eng. Struct.* **46** 87
[28] Ripoll MR, Očenášek J 2009 *Eng Fract Mech* **76** 1485

[29] Izadbakhsh A, Inal K, Mishra R K 2012 *Model Simul Mater Sci Eng* **20**:035016
[30] Lu C, Deng G Y, Tieu A. K, et al. 2011 *Acta Mater.* **59** 3581
[31] Si L Y, Lu C, Huynh N N, et al. 2008 *J Mater Process Technol* **201** 79
[32] Taylor G I 1934 *Proc R Soc A Math Phys Eng Sci* **145** 362
[33] Taylor G I 1934 *Proc R Soc A Math Phys Eng Sci* 145 388
[34] Peirce D, Asaro R J, Needleman A, Park A 1983 *Acta Metall* **31**
[35] Wu T-Y, Bassani J L, Laird C 1991 *Proc.R Soc. A Math. Phys. Eng. Sci.* **435** 1
[36] Bassani J L, Wu T-Y 1991 *Proc. R Soc. A Math. Phys. Eng. Sci.* **435** 21
[37] Deng G Y, Lu C, Tieu A. K, et al. 2010 *J Mater Sci* **45** 4711
[38] Ling G, Havner K 1996 *Int J Plast* **12** 695
[39] Wu P D, Neale IKWI, Giessen E Van Der 1997 *Int J Plast* **12** 1199
[40] Huang Y 1991 "A User-material subroutine incorporating single crystal plasticity in the ABAQUS finite element program. Mech report 178", Division of Engineering and Applied Sciences, Harvard University.
[41] Franciosi P, Berveiller M, Zaoui A, Paris-nord U 1980 *Acta Metall* **28** 273
[42] Akef A., Driver J H 1991 *Mater Sci Eng A* **132** 245
[43] Liu Q, Maurice C, Driver J, Hansen N 1998 *Metal Mater Trans A* **29** 2333
[44] Hafok M, Pippan R 2007 *Sci. Mater.* **56** 757
[45] Méric L, Qailletaud G 1991 *J. Eng. Mater. Technol.* **113** 171
[46] S.Quilici, S.Forest GG, Qailletaud G 1998 *J. Phys.* **8** 325
[47] Rose W, Stüwe H P 1968 *Z Met* **59** 396
[48] Tóth L S, Jonas J J 1989 *Textures and Microstructures* ***10*** *195*
[49] Skrotzki W, Tóth L S, Klöden B, et al. 2008 *Acta Mater* **56** 3439